Fracture Mapping on the Reykjanes Peninsula

Nathaniel Wire[1], Halldór Geirsson[1], and Freysteinn Sigmundsson[1]
[1]University of Iceland

Research Report RH-06-2024
Orkurannsóknasjóður Landsvirkjunar styrk nr. NÝR-30 2024

Reykjavík, Iceland
December 1st, 2024

Contents

1 Samantekt

Takmark þessa verkefnis er að nota InSAR gervihnattamælingar til kortleggja virk misgengi. Gögn frá fjórum TSX römmum sem ná yfir Reykjanesskaga voru greind skv. aðferðum Ducrocq et al. (2024). Alls fengust 57 bylgjuvíxlmyndir milli september 2021 til júlí 2024. Umfangsmestu brotahreyfingarnar tengjast Meradalagosinu 2022, Litla-Hrútsgosinu 2023 og Grindavíkurganginum 2023. Einnig var reiknaður s.k. fasahalli (rúmafleiða bylgjuvíxlmerkis) sem reynist sýna enn fíngerðari hreyfingar; því er fasahalli gagnlegt tæki til að kortleggja misgengisfærslur. Eitt misgengjanna sem hreyfðist liggur um sigdal við Búrfellsgjá nærri Höfuðborgarsvæðinu og voru færslur þar mældar með nákvæmnis hæðarmælingum. Hlutar sniðsins um Búrfellsgjá hafa lækkað um 34 ± 0,3 mm síðan 2012, eða 2,8 mm/ári, sem er mun hraðara sig en áður. Færslur á misgengjum innan sigdalsins tengjast hrinum af grunnri smáskjálftavirkni, í október 2018, mars 2021 og september 2023. Engar kvikuhreyfingar voru nálægt Búrfellsgjá, né í Krýsuvíkurkerfinu sem Búrfellgjá tilheyrir, í október 2018 og september 2023 sem bendir til þess að sumar þessara brotahreyfinga séu af tektónískum uppruna. Verkefnið sýnir notagildi bylgjuvíxlmælinga við kortlagningu virkra misgengja.

2 Abstract

Data from four TerraSAR-X tracks covering the Reykjanes Peninsula were processed to produce 57 interferograms following the methods of Ducrocq et al. (2024) for September 2021 to July 2024. The most extensive fracture movements are associated with the 2022 Meradalir eruption, 2023 Litli-Hrútur eruption, and 2023 Grindavík dike intrusion. Phase gradient calculations (the spatial derivative of the wrapped phase) suggest these data are a useful tool to complement mapping from the wrapped phase, revealing even more subtle features. Some of the fractures in Búrfellsgjá, near the Capital Area, are crossed by a leveling profile that was surveyed in the summer of 2024. Since 2012, portions of the profile have subsided up to 34 ± 0.28 mm, corresponding to a rate of -2.8 mm/yr, substantially greater than that observed in previous years. Displacements along fractures within the Búrfell graben observed with InSAR are associated with bursts of shallow microseismicity in October 2018, March 2021, and September 2023. There have been no recent magma movements in the immediate vicinity of Búrfellsgjá, nor in the broader Krýsuvík fissure swarm to which it belongs, indicating that some of these movements are of tectonic origin. These results demonstrate the utility of X-band radar interferometry for mapping active faults and can be extrapolated to regions with similar features such as Iceland's Northern Volcanic Zone.

3 Introduction

Fault and fracture movements during rifting events have long been recognized as significant mechanism of crustal deformation in Iceland, particularly during the 1975-1984 Krafla Fires and 2014-2015 Holuhraun eruption (Brandsdóttir & Einarsson, 1980; Hjartardóttir et al., 2016; Sigurdsson, 1980). The past several years of activity on the Reykjanes Peninsula have revealed that these are a significant hazard to populated areas, exemplified by the meter-scale displacements produced during the intrusion of a large dike underneath the town of Grindavík on November 10th, 2023 (De Pascale et al., 2024; Sigmundsson et al., 2024). As the Reykjanes Peninsula enters a prolonged period of unrest, understanding the characteristics of these movements and their driving mechanisms is important for hazard assessment. The proximity of this unrest to Iceland's primary airport, critical energy infrastructure, key industrial facilities, and the homes of nearly 300,000 people underscores this. Previous studies have described fractures on the Reykjanes Peninsula and occasional displacements along them, but widespread activation of these structures had not been seen until 2020 (Bufféral et al., 2023; Jónsson, 2009; Keiding et al., 2010; Michalczewska et al., 2014). Ducrocq et al. (2024) describe these movements and a set of methods to map them with TerraSAR-X data, finding that fracture movements are most closely associated with periods of intense seismicity, inflation, and diking.

Structures found on the Reykjanes Peninsula can broadly be classified into two categories: normal faults striking at N(30-45)E° and right-lateral strike slip faults striking N-S. The normal faults can have prominent topographic expressions, with up to 10 meters of throw (Clifton & Kattenhorn, 2006; Clifton & Schlische, 2003). These faults accommodate meter-scale deformation during dike intrusions (Brandsdóttir & Einarsson, 1980; De Pascale et al., 2024; Sigmundsson et al., 2024; Sigurdsson, 1980). The strike-slip faults have generally subtler surface expressions but can produce earthquakes of up to magnitude 6 - 6.5 with magnitudes increasing eastwards (Einarsson et al., 2020; Keiding et al., 2009). Such events occurred in 1929 and 1968 and are likely to recur as plate motion continuously loads faults and volcano-tectonic activity perturbs the stress field (Birgisdóttir, 2023; Einarsson et al., 2020).

As observed by Ducrocq et al. (2024) and others, normal and strike-slip faults on the Reykjanes Peninsula have been observed to exhibit a- and coseismic movements (Feigl et al., 2000; Jónsson, 2009; Keiding et al., 2010; Michalczewska et al., 2014; Pagli et al., 2003). Leveling data collected

from two profiles across portions of the Svartsengi and Krýsuvík fissure swarms, established in the 1960s by Eysteinn Tryggvason, show millimeter to centimeter-scale vertical displacements along faults over periods of years which are variably associated with seismicity (Anell, 2004; Traustadóttir, 2013; Tryggvason, 1968). The Krýsuvík leveling profile crosses multiple normal faults and fractures in the Búrfell graben near Reykjavík, including one identified by Ducrocq et al. (2024) and this study (Traustadóttir, 2013; Tryggvason, 1981). Not only do these data provide clues about the long-term amagmatic deformation processes within Icelandic volcanic systems–no recent magmatic activity has been observed within this portion of the Krýsuvík fissure swarm–but they also have implications for hazard assessment in the Capital Region. The faults within Búrfellsgjá are close to and even extend under portions of suburban Reykjavík, including the Norðlingaholt and Vatnsendi neighborhoods (Fig. 1).

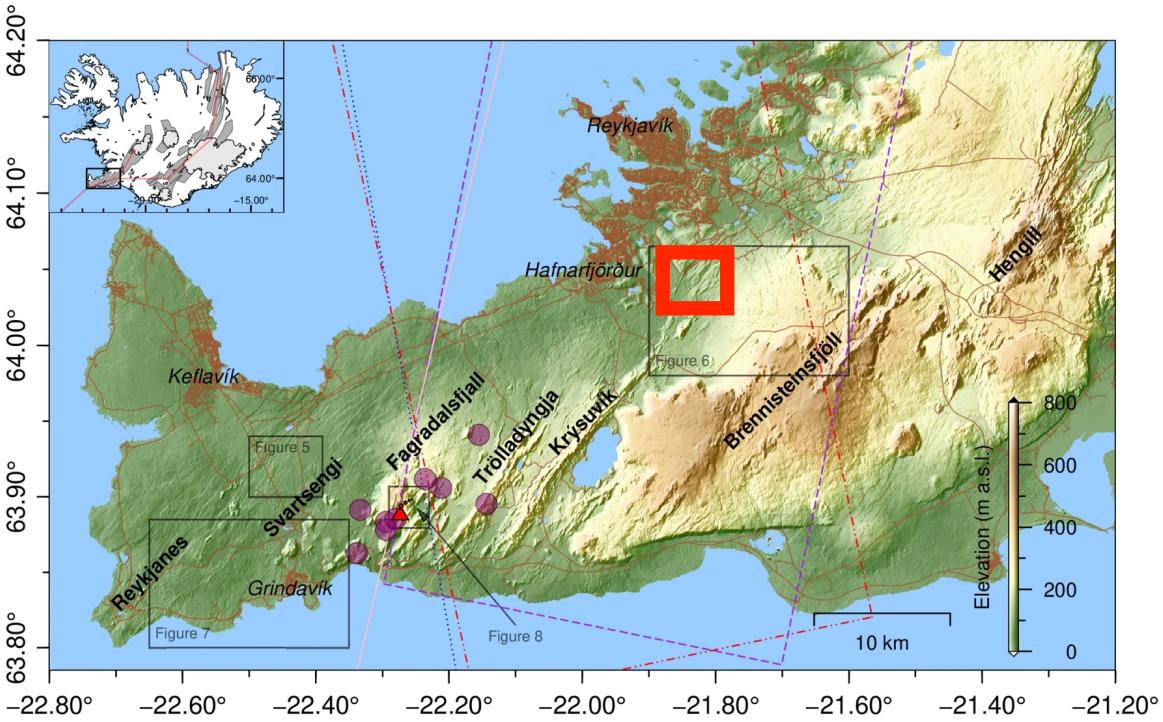

Figure 1: *Map of the Reykjanes Peninsula from Ducrocq et al. (2024). The red rectangle has been added to show the location of Búrfellsgjá.*

This report details an extension of the fault mapping methods described by Ducrocq et al. (2024) to the subsequent period of unrest from September 2021 to July 2024, spanning the December 2021 Fagradalsjall dike intrusion, August 2022 Meradalir eruption, July 2023 Litlí-Hrútur eruption, November 2023 Grindavík dike intrusion, five Sundhnúkur eruptions, and numerous periods of inflation. Phase gradient analysis has proved to be a useful tool in understanding analogous fracture movements during continental strike-slip earthquakes (Fialko, 2004; Fialko et al., 2002; Price & Sandwell, 1998; Xu et al., 2020), so this method was applied to the November 10th dike intrusion. One of the original goals of this study was to use phase gradients to automatically delineate fractures. As preliminary analyses with edge detection algorithms revealed that these images are too noisy to pick out fractures from with any certainty, this was not pursued any further and it was decided to focus on processing InSAR data for wrapped interferograms alone. Results from high-precision geodetic leveling are also presented and compared to InSAR data for the Búrfell graben.

4 Methods

4.1 InSAR

Following the methods described by Ducrocq et al. (2024), TerraSAR-X data from four tracks covering the Reykjanes Peninsula, two ascending (26 and 117) and two descending (110 and 34), were processed using the DORIS and StaMPS softwares (Hooper et al., 2004; Kampes & Usai, 1999). Data was sourced from the Icelandic Volcanoes Supersite (http://geo-gsnl.org/supersites/permanent-supersites/iceland-volcanoes-supersite/) and processed on the University of Iceland's server Dyngja. Once master interferograms were created in DORIS, image pairs with small perpendicular baselines were selected and processed in StaMPS. Of these, interferograms with high coherence spanning periods of high seismicity, inflation, and diking were chosen for mapping (Table 1). Fractures, visible as linear discontinuities in the wrapped phase, were manually mapped in QGIS and subsequently converted from radar to WGS84 coordinates.

Intereferograms for the November 10th, 2023 Grindavík dike intrusion were processed with GMTSAR (Sandwell et al., 2011), chosen for its built-in phase gradient analysis and streamlined geocoding process. A pixel size of 25 m (filter wavelength = 100 m) was chosen to minimize processing time. To test automated fracture delineation with Canny edge detection (Canny, 1986), similar to the methods of Libert et al. (2022), phase gradient images were then run through the openCV `Canny()` function (Bradski, 2000).

4.2 Leveling

Leveling in Búrfellsgjá was conducted over 6 trips in May, June, and July 2024. Most benchmarks are marked with cairns, but several have been lost over the line's 59-year history. Of the 27 benchmarks last surveyed in 2012 (Traustadóttir, 2013), three were unable to be located despite an extensive search: benchmarks 213, 216 and 219. Temporary benchmarks, known as "frogs", were used to span distances between adjacent benchmarks greater than about 50 m. The equipment used for this campaign consists of a Zeiss NiDi 12 Geodetic Digital Level and two Zeiss LD13 Invar rods (Fig. 2). The digital level is first placed on a tripod approximately halfway between the two rods, which are set upon the benchmarks (see Fig. 2). Two pairs of measurements are taken in this configuration to calculate the height difference between the two benchmarks. Measurements are repeated until the measured height differences are within 0.2 millimeters of each other. To account

for any differences between the two rods, the rods are switched, and the process is repeated. If errors are randomly distributed, the uncertainties in the height difference between the first and last benchmark is described by the equation

$$0.2\sqrt{L}$$

where L is the length of the profile in kilometers and the resultant uncertainty is in millimeters (Anell, 2004; Tryggvason, 1968). The length of the Búrfellsgjá profile is 2 kilometers, yielding a minimum uncertainty of ±0.28 mm between benchmarks 258 and 220. Other systemic errors will act to increase this uncertainty.

Figure 2: *Leveling fieldwork in May 2024. The benchmarks in this image span a fracture.*

5 Results

5.1 InSAR

The most widespread fracture movements are associated with the 2022 Meradalir eruption, 2023 Litlí-Hrútur eruption, and November 2023 Grindavík dike intrusion (Fig. 3). Not every fracture in this figure corresponds to these three events–notably those to the southeast of Reykjavík–but the vast majority do, so a three-color scheme was chosen. The distribution of active fractures for each of these events is slightly different. The Meradalir fractures (cyan) include extensive movements along the axis of the plate boundary along with an array of fractures within the fissure swarm of Svartsengi. The Litlí-Hrútur fractures (red) are slightly further north and do not have the same movements along the plate boundary. The fractures active during the Grindavík dike intrusion and subsequent eruptions (purple) have a much wider areal footprint.

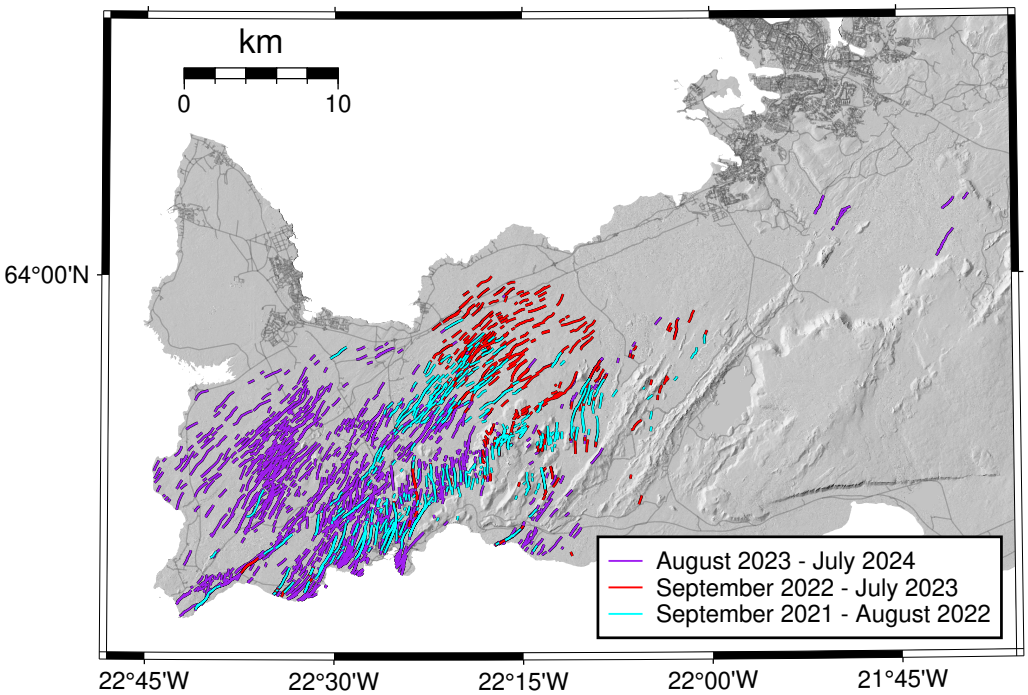

Figure 3: *Fractures active from September 2021 to July 2024. Fractures are separated by the dominant event of each time period, e.g. the 2022 and 2023 Fagradalsfjall eruptions and 2023 Sundhnúkur instrusions and eruptions. Note fracture movements to the southeast of Reykjavík, a considerable distance from the present unrest.*

Fractures active since November 2023 are further west and show clear evolution over time (Fig. 4). While they are centered around the Sundhnúkur/Svartsengi region, the more recent fracture movements have occurred over a much smaller area. Fractures active during the November 10th dike intrusion span approximately 25 km, while those active during the May 2024 eruption span closer to 5 km. Fractures interpreted as active primarily on November 10th are extremely widespread (Fig. 5). These include numerous SW-NE striking fractures to the northwest of the dike, and N-S trending fractures west of Fagradalsfjall. The fractures that run through Grindavík are not mapped here due to poor SAR coherence, but they did move significantly in this event (De Pascale et al., 2024; Sigmundsson et al., 2024). Ducrocq et al. (2024) mapped these structures before November 2023, indicating that they were active before experiencing meter-scale displacements. The amplitudes of most of the displacements are mapped here are much smaller, with an estimated 80 percent showing displacements of less than 10 mm.

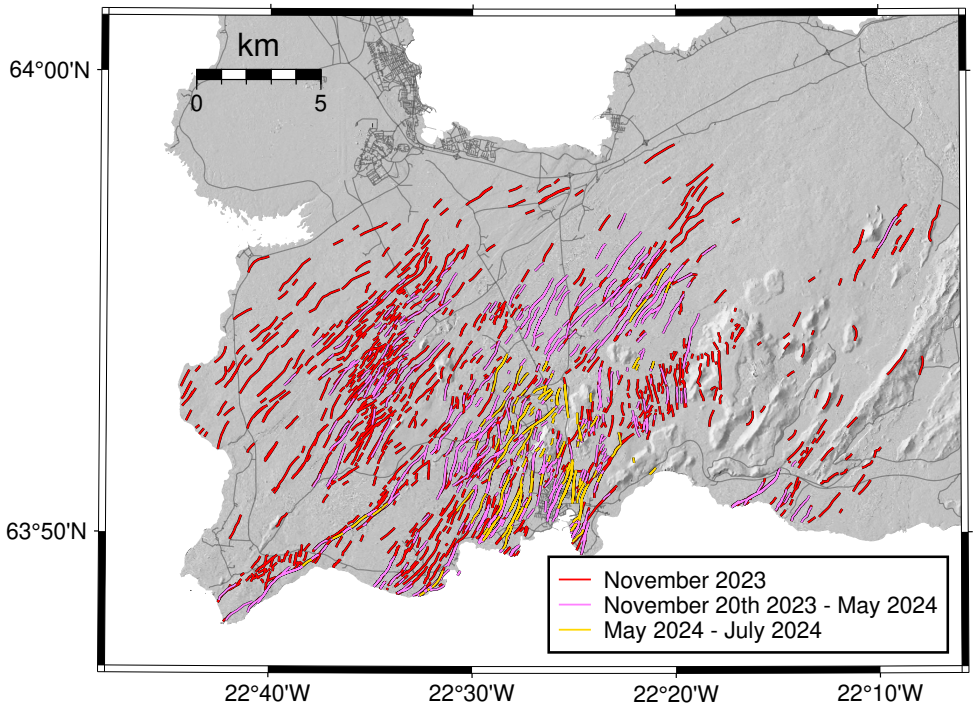

Figure 4: *Fractures active from November 2023 to July 2023. The red fractures are active immediately preceding and during the November 10th dike intrusion, magenta during the following inflation periods and four eruptions (December 2023, January 2024, February 2024, and March 2024), and golden during the May 2024 eruption. Note the decrease in areal extent of fractures with time.*

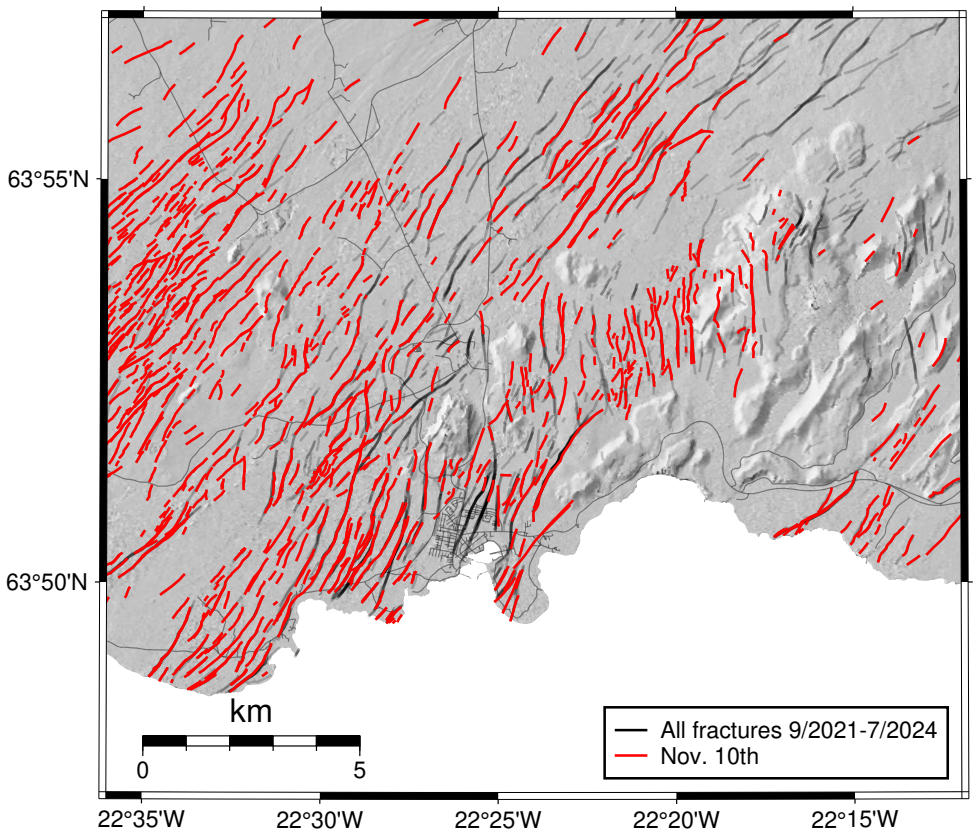

Figure 5: *Fractures mapped from interferograms spanning the November 10th, 2023 dike intrusion and preceding period of inflation (red) compared with all fractures mapped during other periods of eruption/unrest (gray) in the vicinity of Grindavík. The lack of structures in the town of Grindavík for this time period is not real, but rather an artifact of poor image coherence.*

Phase gradient images (Figs. 6 and 7) reveal features not immediately apparent in the wrapped interferograms. However, the phase gradient still suffers from the issues posed by linear topographic features that appear similar to fracture movements as described by Ducrocq et al. (2024), so it is important to evaluate the wrapped phase and gradient in concert with a DEM. Preliminary testing with Canny edge detection (Bradski, 2000; Canny, 1986) revealed that these images were too noisy to accurately delineate fractures in their present form, so this method was not pursued any further. That said, the quality of results for manual mapping indicate that this method is able to reveal fractures just as well, if not better, than the wrapped phase alone. Stacking the phase gradient may increase the signal to noise ratio enough for successful automated fracture delineation.

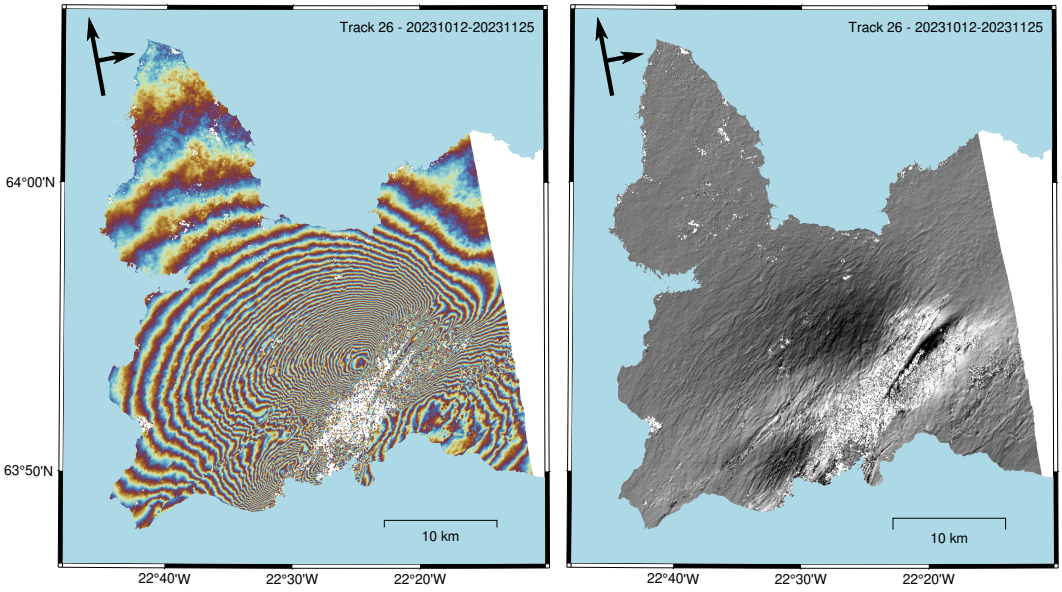

Figure 6: *Wrapped interferogram and phase gradient produced with GMTSAR spanning the Nov. 10th dike intrusion. Larger-wavelength signals to the NW of the dike are related to uplift on the dike flanks and subsidence above the dike and magma source underneath Svartsengi.*

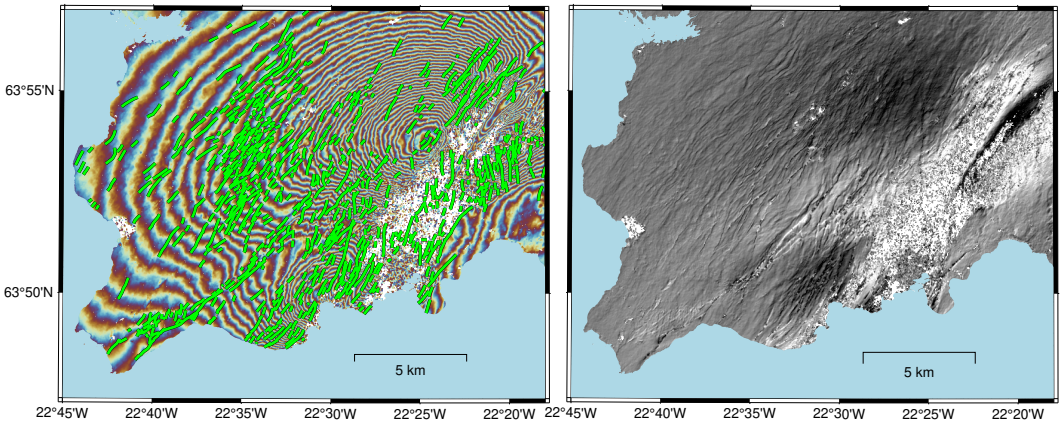

Figure 7: *Comparison of fractures mapped from wrapped phase and phase gradient. Note that phase discontinuities are much easier to spot in the phase gradient image and correlate well with mapped fractures. A different interferogram (using the same two reference images but processed with DORIS/StaMPS instead of GMTSAR) was used for fracture mapping, so there are some fractures located where there is poor coherence in the interferogram shown.*

Movement along the largest fault along the Búrfellsgjá leveling profile is also visible in InSAR data–Ducrocq et al. (2024) identified displacements along this structure in TerraSAR-X data between March 5th, 2021, and March 27th, 2021. Interferograms created this study reveal deformation along this structure during two additional periods—July 11th, 2018, to July 9th, 2019, and September 26th, 2023, to October 24th, 2023 (Appendix Fig. 12). These displacements are generally sub-fringe (<1.5 cm), but clearly visible from both ascending and descending tracks, suggesting that they reflect real fault movements. Interestingly, the most widespread fracture movements within the graben are associated with the February-March 2021 Geldingadalir dike and eruption. All periods of fracture movements are associated with microseismicity within the graben (Fig. 8). Displacements 6-7 km east of Búrfellsgjá associated with earthquake swarms in January and July 2024 (maximum magnitude M_w 3.1) are also observed (Appendix Fig. 13).

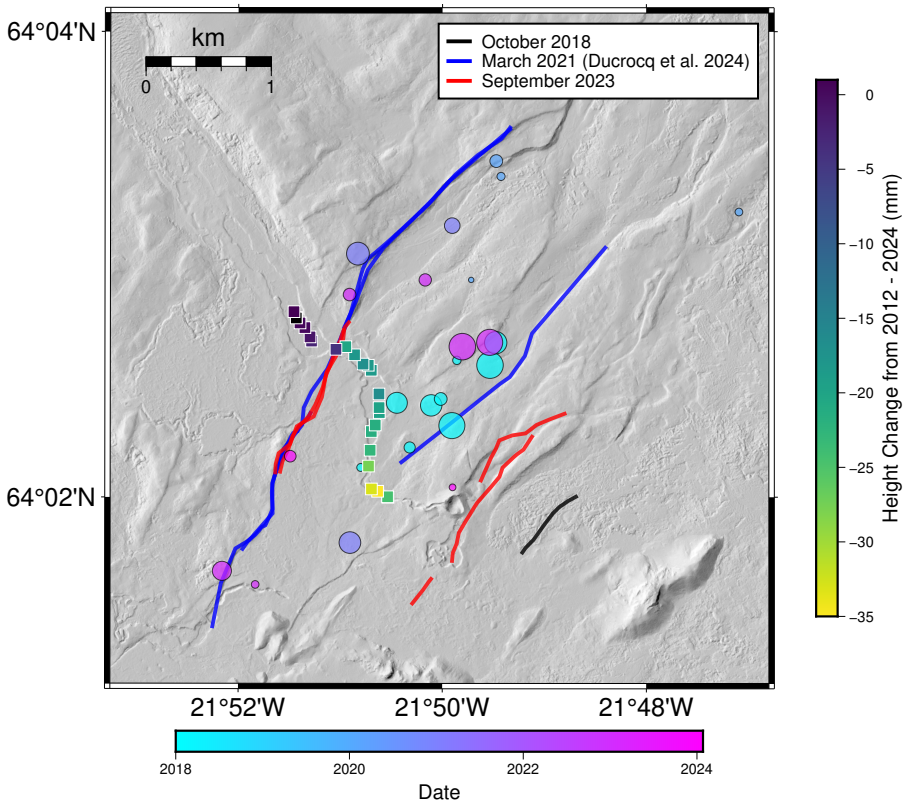

Figure 8: *Height changes, fractures, and seismicity within the Búrfellsgjá graben. The largest displacement between benchmarks occurs across the Hjallar fault on the western side of the graben (Einarsson et al., 2018). None of these earthquakes exceed magnitude 2.4.*

5.2 Leveling

Results from surveys of the Búrfellsgjá profile in 1966, 1980, and 2012 were compared to the data collected in 2024 (Traustadóttir, 2013; Tryggvason, 1968, 1981). The 2012-2024 period shows subsidence up to 34 millimeters relative to the northernmost benchmark, substantially greater than that observed between 1966-1980 and 1980-2012, 12 and 17 millimeters (Ólafsdóttir, 2011; Traustadóttir, 2013). Accordingly, the maximum average subsidence rate for 2012-2024, -2.8 mm/yr, is over three times greater than those measured previously, -0.5 to -0.8 mm/yr (Figs. 9 and 10). The largest vertical displacement measured between benchmarks is 15 mm between points 200 and 202. These two points span the most prominent structure along the profile, the Hjallar Fault (Einarsson et al., 2018), and show similar displacements in 1980-2012—about 10 mm—demonstrating that this structure is active. While the profile crosses the traces of at least five other faults, displacements across these do not exceed 10 mm. There are also faults between benchmarks 218-220 and 215-216, but these do not have a clear surface expression along the profile. Deformation within the graben is heterogeneous in space and time. From the height changes, it can be seen that different faults are active at different times—the zone of greatest subsidence from 1980-2012 is localized between points 200 and 209, while in 1966-1980 and 2012-2024, the greatest subsidence is towards the southeast end of the profile.

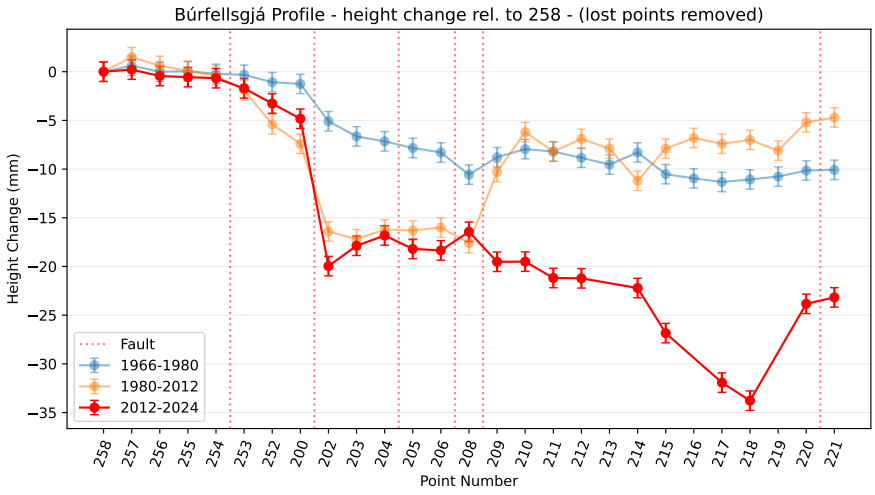

Figure 9: *Height changes of benchmarks for the periods 1966-1980, 1980-2012, and 2012-2024. Faults and fractures are marked by dotted red lines. Horizontal axis not scaled by distance.*

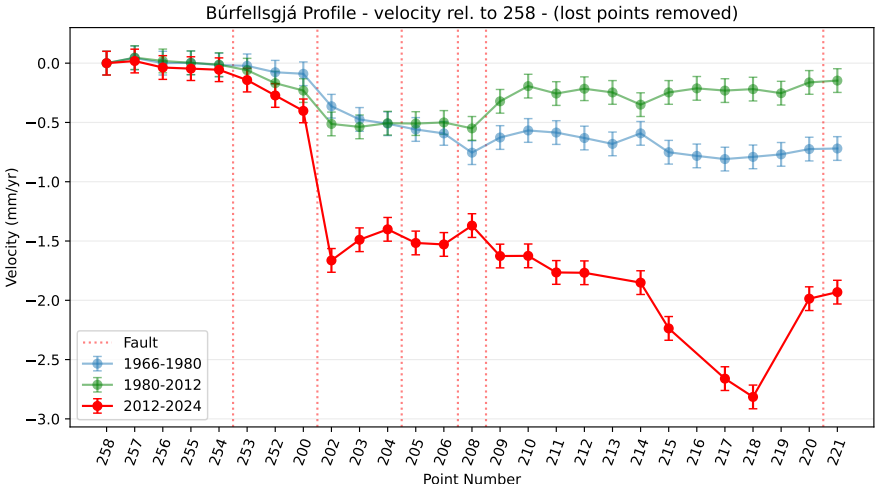

Figure 10: *Average subsidence rates in mm/yr for the same three periods.*

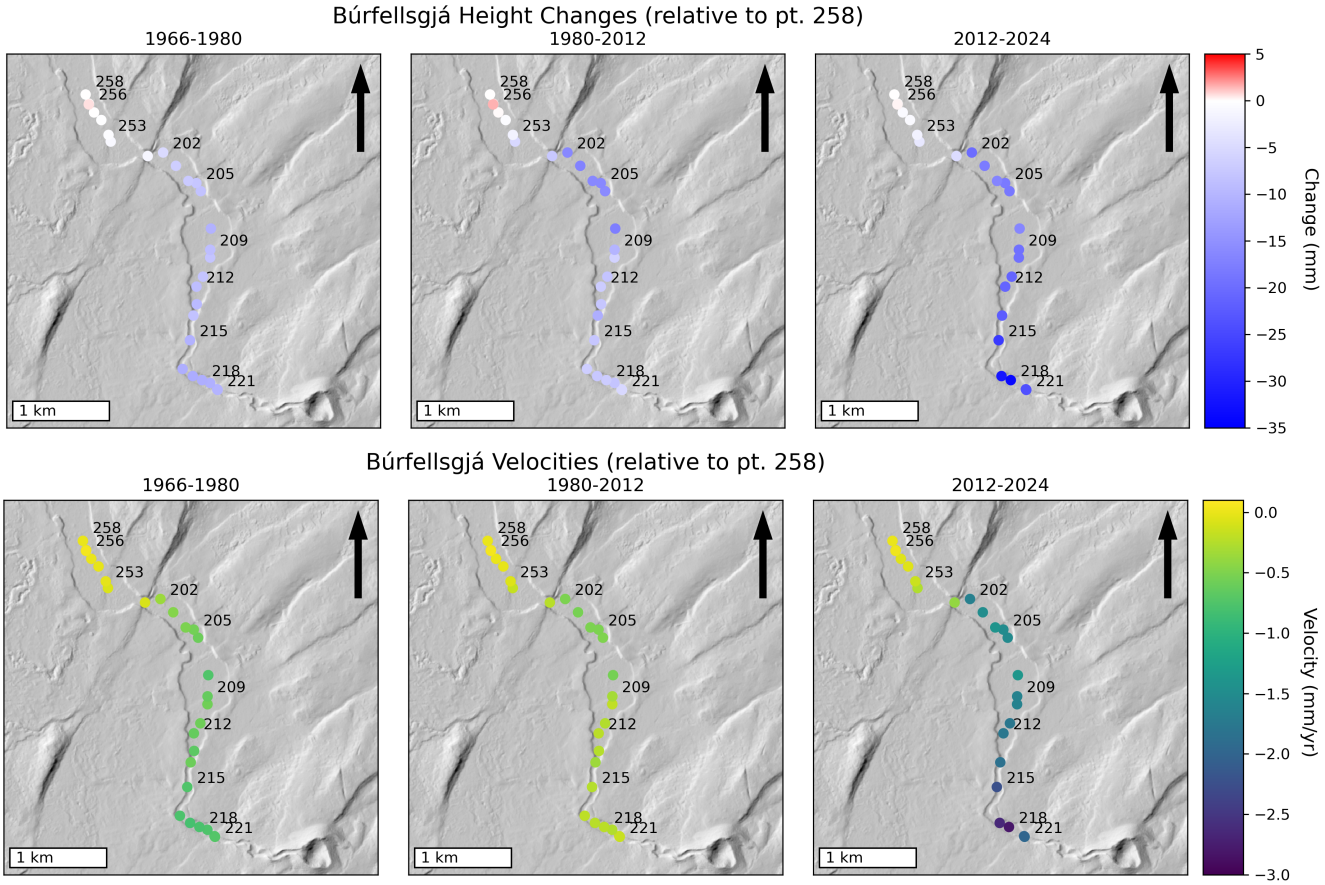

Figure 11: *Map of height changes (top) and velocities (bottom) of benchmarks for the periods 1966-1980, 1980-2012, and 2012-2024.*

6 Discussion

Observations of fracture movements on the Reykjanes Peninsula indicate that these structures are active during both periods of relative quiescence and intense volcano-tectonic unrest, although much more so in the latter.

Two broad categories of fracture movements are observed during diking events: N-S striking along the axis of the plate boundary and N(30°-45)°E striking within the active and adjacent fissure swarms. Note the relative lack of the former during the 2023 Litli-Hrútur eruption (Fig 3). This dike extended further to the north of the previous dikes at Fagradalsfjall, and was associated with very little seismicity along the axis of the plate boundary (Parks et al., 2023; Sigmundsson et al., 2022, 2023). Distal fracture movements in neighboring fissure swarms are only observed during diking events, seemingly only during shallow dike propagation; interferograms spanning periods of inflation or the early stages of dike propagation, such as May 2022, early July 2023, and October 27th, 2023 to November 9th, 2023, lack these distal fracture movements. Many fractures are active to the northwest of the dikes, where co-diking normal stress changes are positive and would ordinarily predict suppressed fracture movements as the fractures are are "clamped". This is apparent during the November 10th diking event, in which fracture movements up to 15 kilometers away from the dike plane are observed. Whether these fractures are weak zones where the dike-induced strain is localized or they are actually slipping in a reverse sense as they are compressed is the subject of ongoing work. The relative roles of dike geometry, stress transfer, strain localization, and tectonic stress in driving fracture movements is unclear, but studying these related phenomena is critical to understand the distribution of fracture movements.

The observation that normal faults within fissure swarms move during amagmatic periods is not new, but explanations of the nature of this deformation vary. Similar displacements and average subsidence rates have been measured along a profile in the Vogar fissure swarm, the largest of which are associated with seismic activity in the early 1970s (Anell, 2004). Aseismic fracture movements have also been observed near Reykjanesvirkjun and have been attributed to a reduction in normal stress due to geothermal reservoir exploitation (Keiding et al., 2010). Similarly, movements along faults in the Þingvellir graben reaching up to 9 cm have been observed with leveling data (Islam et al., 2016). The fact that fracture displacements in Búrfellsgjá only appear in the InSAR data during select periods, with multi-year interferograms outside of these periods show-

ing none, indicates that deformation within Búrfellsgjá is largely episodic. Interestingly, outside of subduction zones, shallow aseismic slip does not appear to be a common phenomenon observed along dip-slip faults (Chen & Bürgmann, 2017). The Icelandic Meteorological Office's depths for the earthquake sequences associated with these fracture movements, downloaded from Skjálftalísa (https://skjalftalisa.vedur.is/index.html#/page/map), are very shallow (<1 km). Similarly, like nearly all other fracture movements observed, fractures withing Búrfellsgjá are sharp discontinuities (Appendix 12). If it is taken that the width of a deformation signal is proportional to the depth of its source (Okada, 1985, 1992), the movements within the graben must be very shallow. These may be coseismic displacements as the uppermost portion of these faults, stressed by ongoing plate spreading, reach a critical stress level and fail. Investigation of these earthquake sequences could provide insight into fault properties and the relative proportions of aseismic and seismic slip in Búrfellsgjá.

7 Conclusions

While only the western Reykjanes Peninsula is presently active, other portions may experience activity in the coming years. The same can be said of other volcanic systems in Iceland. Many have well-developed fissure swarms, so if similar activity were to occur in another region, such as the Northern Volcanic Zone, these fracture mapping methods could be used to monitor the threat that such movements pose to critical infrastructure like the Kárahnjúkar Dam or Þeistareykir and Krafla Power Plants. The occurrence of sporadic movements along fractures on the Reykjanes Peninsula in times of relative quiescence suggests that fractures across Iceland are worth monitoring. Observations of fracture movements in Búrfellsgjá with InSAR and leveling data illustrate the utility of using both remote and field-based techniques to study subtle crustal deformation. InSAR provides spatiotemporal constraints on the deformation, while leveling data provides highly accurate measurements of its vertical component over decadal timescales.

The original goals of this study were to map fractures with wrapped interferograms, create InSAR phase gradients, complete leveling surveys, write a program to automatically delineate fractures, and share the results of this study in a publically accessible manner. While automatic fracture delineation was not achieved in this project, the results of this work do not foreclose it. The successful creation of phase gradient images of diking on the Reykjanes Peninsula indicates that with more time and data, phase gradients can likely be processed in a way to refine the data to a quality sufficient for edge detection. A shapefile of the fractures mapped in this study is available for download on Zenodo: https://doi.org/10.5281/zenodo.14248954.

8 Acknowledgements

This project was funded by Landsvirkjun's Energy Research Fund (Orkurannsóknasjóður Landsvirkjunar) grant number NÝR-30 2024 and conducted at the University of Iceland's Institute of Earth Sciences (Jarðvísindastofnun Háskólans). I would like to thank my advisors for this project: Halldór Geirsson for his assistance with fieldwork and all things deformation, and Freysteinn Sigmundsson for leading helpful discussions on Mondays and his advice on how to contextualize this work. This work would not have been possible without Cécile Ducrocq and Vincent Drouin's guidance and scripts for InSAR processing, in addition to David Sandwell's examples of phase gradient calculations. Finally, I would like to thank to Dani Forester, Cat O'Hara, Sindri Bernholt, Sonja Greiner, Théo Perrot, and Jonas Liebsch for assisting with leveling fieldwork. Figures were created in PyGMT (Uieda et al., 2021).

9 References

Anell, I. (2004). *Subsidence in rift zones: Analyzing results from repeated precision leveling of the Vogar Profile on the Reykjanes Peninsula, Southwest Iceland* [msthesis]. Lund University.

Birgisdóttir, Á. G. (2023). *Coulomb stress changes on the Reykjanes Peninsula from 1998-2022 and earthquake triggering* [BS thesis]. University of Iceland.

Bradski, G. (2000). The OpenCV Library. *Dr. Dobb's Journal of Software Tools*.

Brandsdóttir, B., & Einarsson, P. (1980). Seismological evidence for lateral magma intrusion during the July 1978 deflation of the Krafla volcano in NE-Iceland. *Journal of Geophysics*, *47*(1), 160–165.

Bufféral, S., Panza, E., Mannini, S., Hjartardóttir, Á. R., Nobile, A., Gies, N., Óskarsson, B. V., & Ruch, J. (2023). Surface fractures generated during the 2021 Reykjanes oblique rifting event (SW Iceland). *Bulletin of Volcanology*, *85*(11), 64.

Canny, J. (1986). A Computational Approach to Edge Detection. *IEEE Transactions on Pattern Analysis and Machine Intelligence*, *PAMI-8*(6), 679–698. https://doi.org/10.1109/TPAMI.1986.4767851

Chen, K. H., & Bürgmann, R. (2017). Creeping faults: Good news, bad news? *Reviews of Geophysics*, *55*(2), 282–286.

Clifton, A. E., & Kattenhorn, S. A. (2006). Structural architecture of a highly oblique divergent plate boundary segment. *Tectonophysics*, *419*(1), 27–40. https://doi.org/10.1016/j.tecto.2006.03.016

Clifton, A. E., & Schlische, R. W. (2003). Fracture populations on the Reykjanes Peninsula, Iceland: Comparison with experimental clay models of oblique rifting. *Journal of Geophysical Research: Solid Earth*, *108*, 2001JB000635. https://doi.org/10.1029/2001JB000635

De Pascale, G. P., Fischer, T. J., Moreland, W. M., Geirsson, H., Hrubcová, P., Drouin, V., Forester, D., Payet–Clerc, M., Da Silveira, D. B., Vlček, J., Ófeigsson, B. G., Höskuldsson, Á., Torfadóttir, H. K., Valdimarsdóttir, I. K., Blöndal, B. D. J., Jónsdóttir, I., Jónsson, S., & Thordarson, T. (2024). On the Move: 2023 Observations on Real Time Graben Formation, Grindavík, Iceland. *Geophysical Research Letters*, *51*(14), e2024GL110150. https://doi.org/10.1029/2024GL110150

Ducrocq, C., Árnadóttir, T., Einarsson, P., Jónsson, S., Drouin, V., Geirsson, H., & Hjartardóttir, Á. R. (2024). Widespread fracture movements during a volcano-tectonic unrest: The Reykjanes

Peninsula, Iceland, from 2019–2021 TerraSAR-X interferometry. *Bulletin of Volcanology*, *86*(2), 14. https://doi.org/10.1007/s00445-023-01699-0

Einarsson, P., Hjartardóttir, Á. R., Hreinsdóttir, S., & Imsland, P. (2020). The structure of seismogenic strike-slip faults in the eastern part of the Reykjanes Peninsula Oblique Rift, SW Iceland. *Journal of Volcanology and Geothermal Research*, *391*, 106372. https://doi.org/10.1016/j.jvolgeores.2018.04.029

Einarsson, P., Jóhannesson, H., & Hjartardóttir, Á. R. (2018). Bergsprungur og byggingar á höfuðborgarsvæðinu. *Verktækni–Tímarit VFÍ, bls*, 21–25.

Feigl, K. L., Gasperi, J., Sigmundsson, F., & Rigo, A. (2000). Crustal deformation near Hengill volcano, Iceland 1993–1998: Coupling between magmatic activity and faulting inferred from elastic modeling of satellite radar interferograms. *Journal of Geophysical Research: Solid Earth*, *105*, 25655–25670. https://doi.org/10.1029/2000JB900209

Fialko, Y. (2004). Probing the mechanical properties of seismically active crust with space geodesy: Study of the coseismic deformation due to the 1992 Mw7.3 Landers (southern California) earthquake. *Journal of Geophysical Research: Solid Earth*, *109*(B3).

Fialko, Y., Sandwell, D., Agnew, D., Simons, M., Shearer, P., & Minster, B. (2002). Deformation on nearby faults induced by the 1999 Hector Mine earthquake. *Science*, *297*(5588), 1858–1862.

Hjartardóttir, Á. R., Einarsson, P., Gudmundsson, M. T., & Högnadóttir, T. (2016). Fracture movements and graben subsidence during the 2014 Bárðarbunga dike intrusion in Iceland. *Journal of Volcanology and Geothermal Research*, *310*, 242–252.

Hooper, A., Zebker, H., Segall, P., & Kampes, B. (2004). A new method for measuring deformation on volcanoes and other natural terrains using InSAR persistent scatterers. *Geophysical Research Letters*, *31*(23), 2004GL021737. https://doi.org/10.1029/2004GL021737

Islam, M. T., Sturkell, E., LaFemina, P., Geirsson, H., Sigmundsson, F., & Ólafsson, H. (2016). Continuous subsidence in the Thingvellir rift graben, Iceland: Geodetic observations since 1967 compared to rheological models of plate spreading. *Journal of Geophysical Research: Solid Earth*, *121*(1), 321–338.

Jónsson, S. (2009). Anthropogenic and Natural Deformation on Reykjanes Peninsula, Southwest Iceland, observed using InSAR Time-Series Analysis 1992-2008. *5142*.

Kampes, B., & Usai, S. (1999). Doris: The Delft Object-oriented Radar Interferometric Software.

Keiding, M., Árnadóttir, T., Jónsson, S., Decriem, J., & Hooper, A. (2010). Plate boundary deformation and man-made subsidence around geothermal fields on the Reykjanes Peninsula,

Iceland. *Journal of Volcanology and Geothermal Research*, *194*(4), 139–149. https://doi.org/10.1016/j.jvolgeores.2010.04.011

Keiding, M., Lund, B., & Árnadóttir, T. (2009). Earthquakes, stress, and strain along an obliquely divergent plate boundary: Reykjanes Peninsula, southwest Iceland. *Journal of Geophysical Research: Solid Earth*, *114*, 2008JB006253. https://doi.org/10.1029/2008JB006253

Libert, L., Wuite, J., & Nagler, T. (2022). Automatic delineation of cracks with Sentinel-1 interferometry for monitoring ice shelf damage and calving. *The Cryosphere*, *16*(4), 1523–1542. https://doi.org/10.5194/tc-16-1523-2022

Michalczewska, K., Hreinsdóttir, S., Stéphanie, D., & Sigmundsson, F. (2014). *Crustal deformation on the Western Reykjanes Peninsula 2009 to 2014 mapped by InSAR and GPS measurements* (JH1401). Institute of Earth Sciences. University of Iceland.

Okada, Y. (1985). Surface deformation due to shear and tensile faults in a half-space. *Bulletin of the seismological society of America*, *75*(4), 1135–1154.

Okada, Y. (1992). Internal deformation due to shear and tensile faults in a half-space. *Bulletin of the seismological society of America*, *82*(2), 1018–1040.

Ólafsdóttir, R. (2011). *Halla- og hæðarmælingar á íslandi sem framkvæmdar hafa verið af eysteini tryggvasyni og starfsmönnum norrænu eldfjallastöðvarinnar og jarðvísindastofnunar háskólans*. Jarðvísindastofnun Háskólans. University of Iceland.

Pagli, C., Pedersen, R., Sigmundsson, F., & Feigl, K. L. (2003). Triggered fault slip on june 17, 2000 on the reykjanes peninsula, sw-iceland captured by radar interferometry. *Geophysical Research Letters*, *30*(6).

Parks, M., Sigmundsson, F., Drouin, V., Hjartardóttir, Á. R., Geirsson, H., Hooper, A., Vogfjörd, K. S., Ófeigsson, B. G., Hreinsdóttir, S., Jensen, E. H., Einarsson, P., Barsotti, S., & Fridriksdóttir, H. M. (2023). Deformation, seismicity, and monitoring response preceding and during the 2022 fagradalsfjall eruption, iceland. *Bulletin of Volcanology*, *85*(10), 60. https://doi.org/10.1007/s00445-023-01671-y

Price, E. J., & Sandwell, D. T. (1998). Small-scale deformations associated with the 1992 Landers, california, earthquake mapped by synthetic aperture radar interferometry phase gradients. *Journal of Geophysical Research: Solid Earth*, *103*, 27001–27016. https://doi.org/10.1029/98JB01821

Sandwell, D., Mellors, R., Tong, X., Wei, M., & Wessel, P. (2011). GMTSAR: An InSAR processing system based on generic mapping tools.

Sigmundsson, F., Parks, M., Geirsson, H., Vogfjord, K. S., Drouin, V., Tolpekin, V., Wollersheim, M., Ofeigsson, B., Hooper, A. J., Hjartardottir, A. R., et al. (2023). The 4th Diking Event of the Fagradalsfjall Rifting Episode (2021-?) in July 2023: Geodetic and Seismic Imaging of the Dike Propagation and Effects of Imposed Stresses on the Dike and the Associated Eruption. *AGU Fall Meeting Abstracts*, *2023*(7), V41G–07.

Sigmundsson, F., Parks, M., Geirsson, H., Hooper, A., Drouin, V., Vogfjörd, K. S., Ófeigsson, B. G., Greiner, S. H. M., Yang, Y., Lanzi, C., De Pascale, G. P., Jónsdóttir, K., Hreinsdóttir, S., Tolpekin, V., Friðriksdóttir, H. M., Einarsson, P., & Barsotti, S. (2024). Fracturing and tectonic stress drive ultrarapid magma flow into dikes. *Science*, *383*(6688), 1228–1235. https://doi.org/10.1126/science.adn2838

Sigmundsson, F., Parks, M., Hooper, A., Geirsson, H., Vogfjörd, K. S., Drouin, V., Ófeigsson, B. G., Hreinsdóttir, S., Hjaltadóttir, S., Jónsdóttir, K., Einarsson, P., Barsotti, S., Horálek, J., & Ágústsdóttir, T. (2022). Deformation and seismicity decline before the 2021 Fagradalsfjall eruption. *Nature*, *609*(7927), 523–528. https://doi.org/10.1038/s41586-022-05083-4

Sigurdsson, O. (1980). Surface deformation of the Krafla Fissure Swarm in two rifting events. *Journal of Geophysics*, *47*(1), 154–159.

Traustadóttir, M. (2013). *Hallamælingar í búrfellsgjá sumarið 2012* [bsthesis]. University of Iceland.

Tryggvason, E. (1968). Measurement of surface deformation in iceland by precision leveling. *Journal of Geophysical Research*, *73*(22), 7039–7050.

Tryggvason, E. (1981). *VERTICAL COMPONENT OF GROUND DEFORMATION IN SOUTHWEST- AND NORTH-ICELAND Results of levelings in 1976 and 1980*. Nordic Volcanological Institute, University of Iceland. Reykjavík, Iceland.

Uieda, L., Tian, D., Leong, W. J., Toney, L., Schlitzer, W., Grund, M., Newton, D., Ziebarth, M., Jones, M., & Wessel, P. (2021). PyGMT: A Python interface for the generic mapping tools.

Xu, X., Sandwell, D. T., Ward, L. A., Milliner, C. W. D., Smith-Konter, B. R., Fang, P., & Bock, Y. (2020). Surface deformation associated with fractures near the 2019 Ridgecrest earthquake sequence. *Science*, *370*(6516), 605–608. https://doi.org/10.1126/science.abd1690

10 Appendix

Table 1: List of interferograms used for fracture mapping. B_{Par} and B_{Perp} refer to the parallel and perpendicular distance between acquisitions while H_a (m) refers to the shift in B_{Perp} necessary to generate one fringe of deformation. Table is continued on the next page.

Track	Primary Image	Secondary Image	B_{Par} (m)	B_{Perp} (m)	H_a (m)
26	20231012	20231125	49.90	57.23	-126.85
26	20230705	20231001	-82.76	-114.964	63.14
26	20231125	20240108	-0.91	-13.05	556.172
26	20231217	20240405	-79.68	-4.12	1831.76
26	20240108	20240221	-86.8	-85.66	84.76
26	20240221	20240405	-22.16	68.30	-106.257
26	20240314	20240405	63.85	157.54	-46.08
26	20231206	20231217	112.33	136.47	-53.20
26	20240530	20240724	56.63	-27.64	262.57
26	20240519	20240621	-93.55	-26.04	278.67
26	20240405	20240530	118.51	24.33	-299.28
26	20230602	20230705	46.52	-72.34	100.31
26	20230430	20230705	49.19	35.06	-207.02
26	20220809	20221116	56.75	-16.59	437.61
26	20220809	20221105	108.49	73.49	-98.82
26	20220809	20220922	39.66	61.24	-118.53
26	20220729	20220809	-125.59	-146.09	49.70
26	20220421	20220604	2.76	-114.60	63.33
26	20211221	20220513	463.28	-90.88	80.01
110	20220427	20220826	76.62	68.69	-75.07
110	20220530	20220826	-15.97	51.60	-99.90
110	20210908	20211113	-139.35	-20.91	248.63
110	20211022	20211227	136.61	21.08	-245.94
110	20211227	20220530	10.56	-29.69	173.64
110	20230630	20230802	-57.43	-31.61	163.29
110	20221203	20230425	-76.99	15.77	-327.28
110	20230711	20231007	-175.07	47.05	-109.68
110	20230802	20231109	55.36	26.35	-195.8
110	20231007	20231120	233.67	33.77	-153.97
110	20231120	20240503	-56.44	22.84	-225.85
110	20231212	20240103	-218.83	17.75	-292.19
110	20240114	20240525	-3.91	42.76	-120.58
110	20240227	20240320	-18.14	-25.49	202.29
110	20240411	20240525	73.70	-22.57	228.50
110	20240411	20240719	-18.66	11.60	-444.12
110	20240525	20240719	-92.35	17.71	-291.67
110	20240616	20240719	-52.75	22.38	-230.32

Track	Primary Image	Secondary Image	B_{Par} (m)	B_{Perp} (m)	H_a (m)
34	20220810	20220923	-33.54	16.62	-386.10
34	20211108	20220422	151.15	-44.81	143.17
34	20210812	20211006	24.35	-66.95	95.80
34	20220719	20220821	55.87	-19.30	332.47
34	20230808	20231024	-27.39	-98.86	64.89
34	20231024	20231126	-103.22	157.63	-40.69
34	20231126	20240520	18.32	9.18	-699.08
34	20240520	20240703	164.72	-59.93	107.07
34	20230523	20230808	55.38	33.63	-190.92
34	20230523	20230706	78.75	-39.48	162.49
117	20230926	20231120	-32.01	55.57	-108.01
117	20240422	20240719	-94.02	-4.29	1508.33
117	20240114	20240411	-52.57	-0.33	-727.01
117	20231007	20231120	-54.09	36.39	-165.08
117	20230630	20231109	-119.49	-112.74	53.30
117	20230517	20230630	101.87	-24.41	246.19
117	20220804	20220917	-46.27	12.22	-491.77
117	20220724	20220815	-52.13	-91.15	65.86
117	20211011	20211227	-357.50	-52.85	113.67
117	20181007	20191007	0.41	26.19	-233.67

Table 2: Leveling benchmarks (from S to N), WGS84 coordinates from Traustadóttir (2013), and measured heights in cm for 2024 relative to benchmark 200. Benchmarks 219, 216, and 213 were not found but the coordinates have been included.

Benchmark No.	Lat	Lon	Height (cm)
221	64.033333	-21.842222	214.6855
220	64.033361	-21.842278	202.71925
219	64.033639	-21.843056	Not found
218	64.03375	-21.843917	26.025
217	64.033917	-21.844917	60.34025
216	64.034222	-21.846028	Not found
215	64.035556	-21.845389	-249.9915
214	64.036694	-21.845139	-393.45825
213	64.037222	-21.844833	Not found
212	64.038028	-21.844944	-425.6385
211	64.0385	-21.844306	-390.39525
210	64.039389	-21.843639	-379.11725
209	64.03975	-21.843667	-463.329
208	64.040722	-21.843694	-522.261
206	64.042417	-21.844944	-647.94175
205	64.042778	-21.845444	-722.82675
204	64.042861	-21.846306	-516.81875
203	64.043528	-21.847694	-387.58425
202	64.044111	-21.849111	-307.32325
200	64.043917	-21.850722	0
252	64.044503	-21.85471	-3.454
253	64.044806	-21.854972	132.61175
254	64.045472	-21.855806	147.42625
255	64.045806	-21.856611	214.7475
256	64.046194	-21.857194	230.84875
257	64.0461627	-21.857213	225.8545
258	64.046611	-21.857583	212.9829

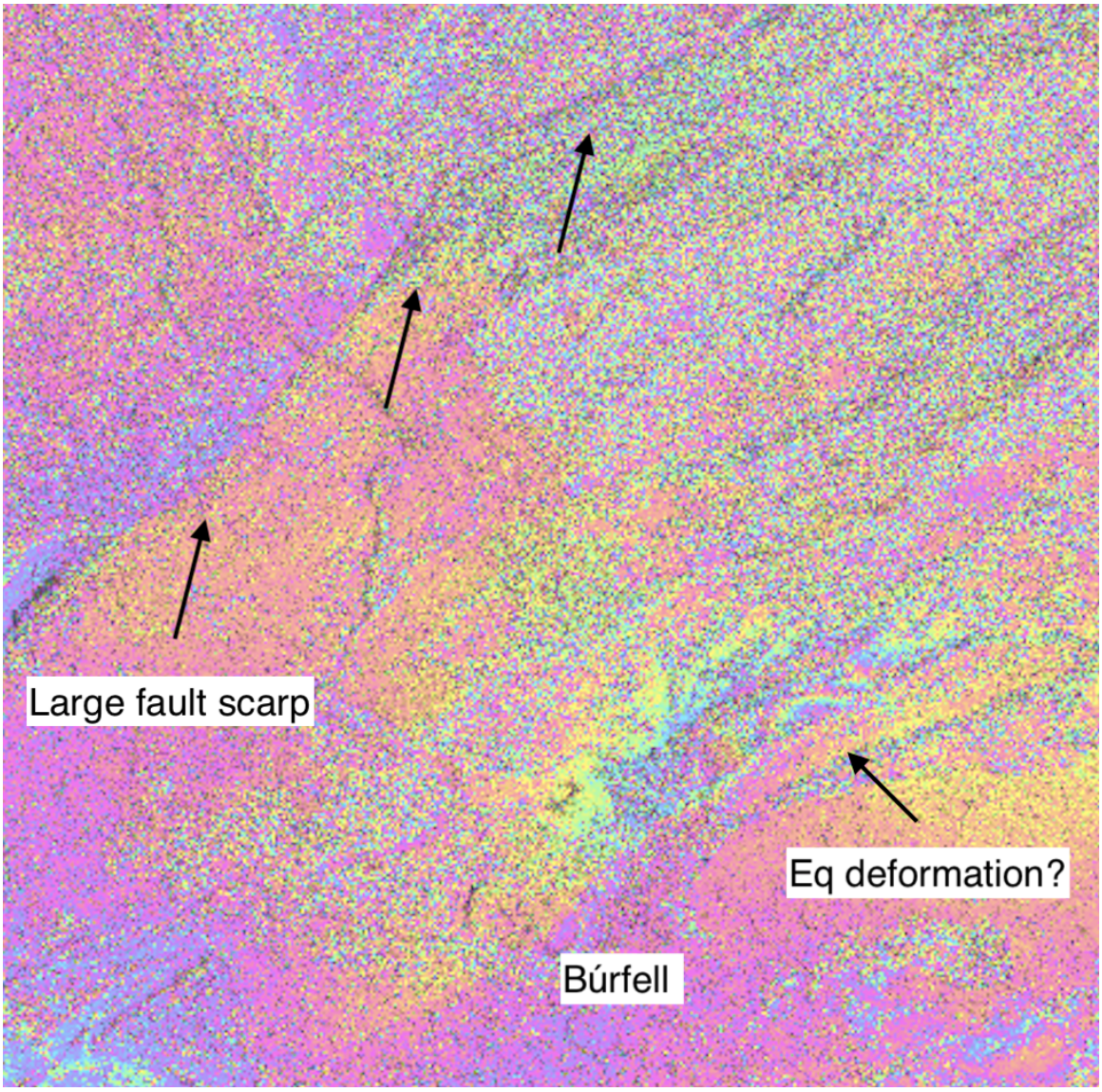

Figure 12: *Subtle fracture movements within Búrfellsgjá from an interferogram spanning September 26, 2023 to November 20th, 2023.*

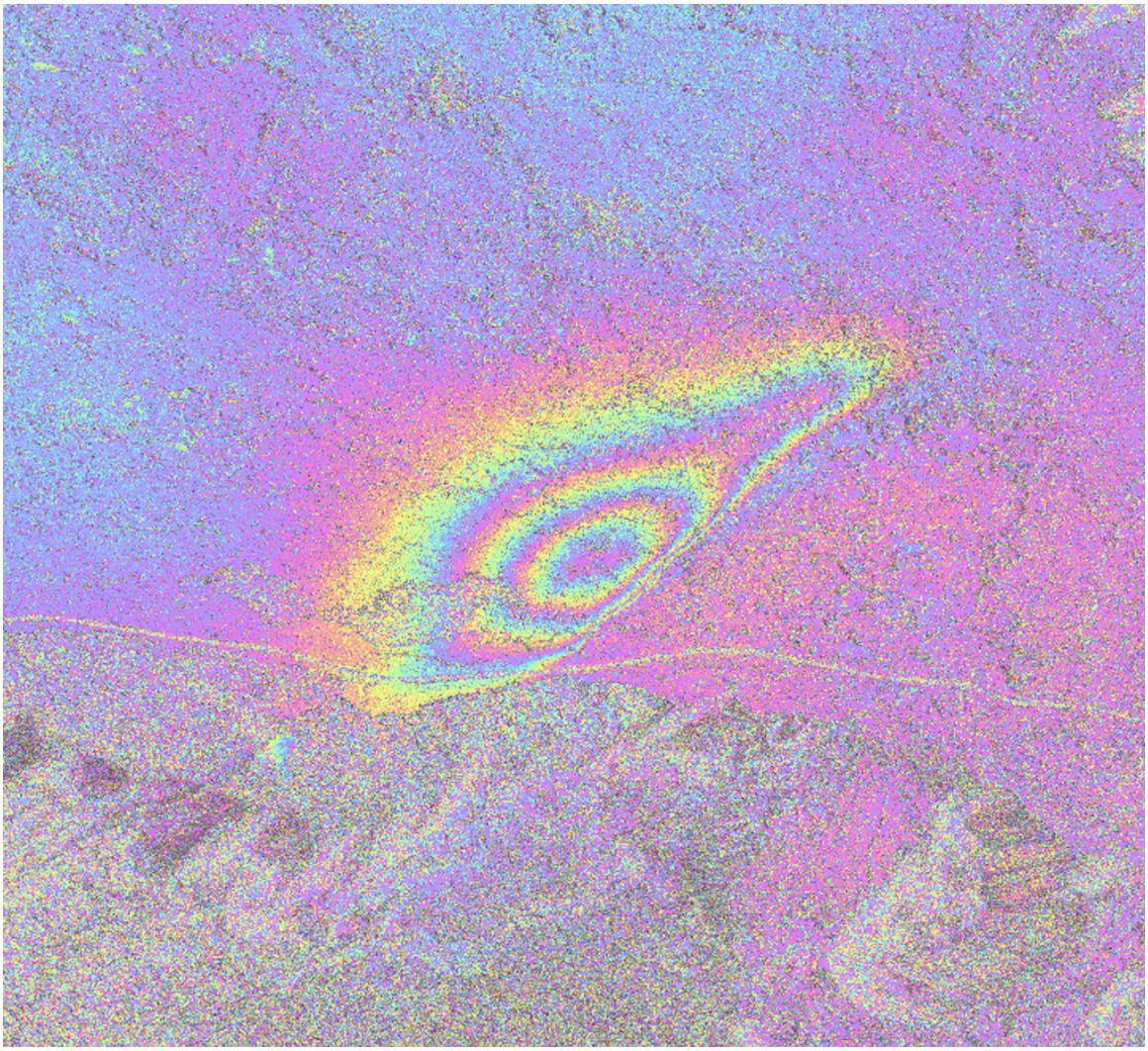

Figure 13: *Deformation (maximum 4-5 cm) associated with an earthquake swarm in January 2024 to the NW of Stóra-Kóngsfell. The E-W linear feature is Bláfjallavegur, and the signal is about 1.5 km long.*